Electronic Supplementary Information

Development of a new Lindqvist-like Fe_6 cluster secondary building unit for MOFs

Li-Dan Lin,[a] Zhong Li,[a] Dan Zhao,[b] Jin-Hua Liu,[a] Xin-Xiong Li*[a] and Shou-Tian Zheng*[a]

[a]State Key Laboratory of Photocatalysis on Energy and Environment, College of Chemistry, Fuzhou University, Fuzhou, Fujian 350108, China.

[b]Fuqing Branch of Fujian Normal University, Fuqing, Fujian, 350300, China.

This file includes:

Section S1 Experimental Section

Materials: All chemicals were commercially purchased and used without further purification. The ligand H_3L[1] was synthesized according literatures procedure.

Instruments: Elemental analyses of C, H and N were carried out with a Vario EL III elemental analyzer. IR spectra were recorded on an Opus Vertex 70 FT-IR infrared spectrophotometer in the range of 450-4000 cm^{-1}. X-ray photoelectron spectroscopy (XPS) was carried out on an ESCALAB 250 spectrometer with an Al-Ka (1486.6 eV) achromatic X-ray source. Thermogravimetric analysis was performed on a Mettler Toledo TGA/SDTA 851e analyzer under an air-flow atmosphere with a heating rate of 10 ºC/min in the temperature of 30-800 ºC. Powder XRD patterns were obtained using a Philips X'Pert-MPD diffractometer with CuKα radiation (λ = 1.54056 Å).

Gas adsorption measurement: N_2 and CO_2 adsorption isotherm were recorded in the ASAP (Accelerated Surface Area and Porosimetry) 2020 System. Before measurement, **1** and **3** was activated by soaking the crystals in acetonitrile for three days to exchange solvent molecules and then degassed at 333K for 12 h under vacuum. Unfortunately, the framework of **3** suffered collapse during the activation process.

Proton-conducting measurement: Ac impedance measurements were carried out with a zennium/IM6 IMPEDANCE/GAINPHASE analyzer over the frequency range from 0.1 Hz to 5 MHz with an applied voltage of 50 mV. The relative humidity was controlled by a STIK Corp CIHI-150B incubator. The samples were pressed to form a cylindrical pellet of crystalline powder sample (~1.2 mm thickness ×5 mm ϕ) coated with C-pressed electrodes. Two silver electrodes were attached to both sides of pellet to form four end terminals (quasi-four-probe method). The bulk conductivity was estimated by semicircle fittings of Nyquist plots.

Magnetic properties measurement: Variable temperature susceptibility measurements were carried out in the temperature range 2-300 K with a scan rate of 2 K/min at a magnetic field of 0.1 T on polycrystalline samples with a Quantum Design PPMS-9T magnetometer. The experimental susceptibilities were corrected for the Pascal's constants.

Synthesis of $[NH_2(CH_3)_2]Fe^{III}_6OCl_6(L)_4Fe^{II}Cl_2(NMF)_2[Fe^{II}(NMF)_2(H_2O)_2]_{0.5}\cdot 4NMF\cdot 4H_2O$ (1) A 20 mL vial containing $SbCl_3$ (0.032 g, 0.14 mmol), $FeCl_3$ (0.025 g, 0.15 mmol), H_3L (0.018 g, 0.10 mmol), NH_4Cl (0.030 g, 0.56 mmol), N-Methylformamide (NMF, 5.0 mL) and 1,4-dioxane (1.0 mL) was sealed and heated in an oven at 100 ºC for 72 h, then cooled to room temperature. Large brown block crystals were obtained after washed with fresh acetonitrile. The yield was about 32% based on $FeCl_3$. Elemental analysis calcd (%) for $H_{93}C_{52}N_{12}O_{25}Cl_8Fe_{7.5}$ (M_r = 1988.82): C, 31.40; H, 4.71; N, 8.45. Found: C, 31.46; H, 4.53; N, 8.38. IR (KBr, cm^{-1}): 3319 (w), 3071 (w), 2870 (w), 1647 (s), 1534 (w), 1462 (w), 1359 (m), 1230 (w), 1154 (w), 1062 (vs), 926 (s), 819 (w), 775 (w), 678 (w), 510 (vs).

Synthesis of $Fe^{III}_6OCl_6(L)_4Fe^{II}(NMF)_2\cdot4NMF\cdot6H_2O$ (2): A 20 mL vial containing $SbCl_3$ (0.032 g, 0.14 mmol), $FeCl_3$ (0.023 g, 0.14 mmol), H_3L(0.018 g, 0.10 mmol), NH_4Cl (0.032 g, 0.60 mmol), isonicotinic acid (0.06 g, 0.49 mmol) and N-Methylformamide (NMF) (5.0 mL) was sealed and heated in an oven at 100°C for 72h, then cooled to room temperature. Brown flake crystals were obtained after cooling to room temperature. The yield was about 12% based on $FeCl_3$. Elemental analysis calcd (%) for $H_{82}C_{48}N_{10}O_{25}Cl_6Fe_7$ (M_r = 1802.85): C, 31.98; H, 4.58; N, 7.77. Found: C, 31.76; H, 4.42; N, 7.72. IR (KBr, cm^{-1}): 3333 (w), 3061 (w), 2858 (w), 1647 (s), 1541 (w), 1465 (w), 1373 (m), 1226 (w), 1156 (w), 1058 (vs), 920 (s), 827 (w), 764 (w), 687 (w), 512 (vs).

Synthesis of $Fe^{III}_6OCl_6(L)_4(CuI)[Fe^{II}(NMF)_2(H_2O)_2]\cdot7NMF\cdot9H_2O$ (3): A 20 mL vial containing $SbCl_3$ (0.032 g, 0.14 mmol), $FeCl_3$ (0.025 g, 0.15 mmol), H_3L (0.018 g, 0.10 mmol), CuI (0.019g, 0.1 mmol) NH_4Cl (0.03 g, 0.56 mmol) and N-Methylformamide (NMF, 5.0 mL) was sealed and heated in an oven at 100°C for 72 h, then cooled to room temperature. Brown block crystals were obtained after washed with fresh acetonitrile. The yield was about 42% based on $FeCl_3$. Elemental analysis calcd (%) for $H_{107}C_{54}N_{13}O_{33}Cl_6Fe_7CuI$ (M_r = 2260.58): C, 28.69; H, 4.77; N, 8.05. Found: C, 28.49; H, 4.57; N, 8.16. IR (KBr, cm^{-1}): 3319 (w), 3071 (w), 2865 (w), 1646 (s), 1538 (w), 1462 (w), 1376 (m), 1235 (w), 1154 (w), 1062 (vs), 932 (s), 819 (w), 765 (w), 678 (w), 515 (vs).

Single-crystal structure analyses: Single-crystal X-ray diffraction data for **1-3** were collected on a Bruker APEX II diffractometer at 150 K equipped with a fine focus, 2.0 kW sealed tube X-ray source (MoK radiation, λ = 0.71073 Å) operating at 50 kV and 30 mA. The program SADABS was used for the absorption correction. The structures were solved by the direct method and refined on F^2 by full-matrix least-squares methods using the SHELX-2013 program package. All hydrogen atoms attached to carbon atoms were generated geometrically. Due to the highly porous characteristic of structures, the charge compensation anions and guest solvent molecules cannot be definitely mapped by single-crystal X-ray diffractions. The residual electron density that could not sensibly be modeled as solvent or cations were removed *via* application of the SQUEEZE[2] function in PLATON. The final formula of **1-3** were determined by the combination of single-crystal X-ray diffractions with the elemental analysis, thermogravimetric analysis (Fig. S21) and charge balance. Crystallographic data and structure refinements for **1-3** are summarized in Table S1. CCDC **1** (1915563), **2** (1915565) and **3** (1915564) involves the supplementary crystallographic data for this paper. These data can be obtained free of charge from The Cambridge Crystallographic Data Centre *via* www.ccdc.cam.ac.uk/data_request/cif.

Section S2 Additional Tables

Table S1 X-ray crystallographic data for **1-3**

	1	**2**	**3**
Empirical formula	$C_{52}H_{92}O_{25}N_{12}Cl_8Fe_{7.5}$	$C_{48}H_{82}O_{25}N_{10}Cl_6Fe_7$	$C_{54}H_{107}O_{33}N_{13}Cl_6Fe_7CuI$
Formula weight	1987.81	1802.85	2260.58
Crystal system	Triclinic	Orthorhombic	Monoclinic
Space group	*P*1	*Ccca*	*P*21/*c*
a (Å)	11.4330(16)	22.375(2)	11.4027(18)
b (Å)	14.879(2)	23.965(2)	54.461(8)
c (Å)	25.862(4)	27.502(3)	18.009(3)
α (°)	88.484(3)	90	90
β (°)	84.890(3)	90	112.514(8)
γ (°)	77.817(3)	90	90
V (Å^3)	4283.1(11)	14747(2)	10331(3)
Z	2	8	4
F(000)	1644	5871	3327
ρ_{calcd}(g cm^{-3})	1.265	1.312	1.079
Temperature (K)	175(2)	175(2)	175(2)
μ(mm^{-1})	1.532	1.605	1.648
Refl. Collected	32542	33142	33580
Independent refl.	14985	6522	17877
Parameters	701	337	700
GOF on F^2	1.030	1.004	1.009
Final *R* indices (I= 2σ(I))	R_1=0.0765 wR_2=0.2294	R_1=0.0375 wR_2=0.1090	R_1=0.0964 wR_2=0.2490
R indices (all data)	R_1= 0.0997 wR_2= 0.2433	R_1=0.0423 wR_2=0.1114	R_1=0.1313 wR_2=0.2619

$R_1 = \sum||F_o| - |F_c||/\sum|F_o|$. $wR_2 = [\sum w(F_o^2 - F_c^2)^2/\sum w(F_o^2)^2]^{1/2}$; $w = 1/[\sigma^2(F_o^2) + (xP)^2 + yP]$, $P = (F_o^2 + 2F_c^2)/3$, where x = 0.164560, y = 0 for **1**; x = 0.048900, y = 100.833911 for **2**; x = 0.178700, y = 27.248402 for **3**.

Table S2 The bond valence sum calculations for **1**

Atoms	*Calcd for Fe^{II}*	*Calcd for Fe^{III}*	*Oxidation*
Fe1	**2.815**	**3.020**	***Fe^{III}***
Fe2	**2.791**	**2.994**	***Fe^{III}***
Fe3	**2.754**	**2.961**	***Fe^{III}***
Fe4	**2.816**	**3.022**	***Fe^{III}***
Fe5	**2.788**	**2.990**	***Fe^{III}***
Fe6	**2.770**	**2.971**	***Fe^{III}***
Fe7	**2.149**	**2.278**	***Fe^{II}***
Fe8	**1.901**	**2.004**	***Fe^{II}***

Table S3 The bond valence sum calculations for **2**

Atoms	*Calcd for Fe^{II}*	*Calcd for Fe^{III}*	*Oxidation*
Fe1	**2.741**	**3.020**	***Fe^{III}***
Fe2	**2.765**	**2.994**	***Fe^{III}***
Fe3	**2.848**	**2.961**	***Fe^{III}***
Fe4	**2.823**	**3.022**	***Fe^{III}***
Fe5	**1.730**	**1.783**	***Fe^{II}***

Table S4 The bond valence sum calculations for **3**

Atoms	*Calcd for Fe^{II}*	*Calcd for Fe^{III}*	*Oxidation*
Fe1	**2.723**	**2.922**	***Fe^{III}***
Fe2	**2.728**	**2.928**	***Fe^{III}***
Fe3	**2.919**	**3.077**	***Fe^{III}***
Fe4	**2.703**	**2.900**	***Fe^{III}***
Fe5	**2.796**	**2.999**	***Fe^{III}***
Fe6	**2.709**	**2.907**	***Fe^{III}***
Fe7	**1.723**	**1.801**	***Fe^{II}***

Table S5 The proton conductivity values of reported MOFs up to 10^{-3} S cm^{-1}:

Compounds	Proton Conductivity Value (S cm^{-1})	Conditions	Activation Energy (eV)	Ref.
1	2.84×10^{-2}	85 °C, 98% RH	0.24	This
2	6.37×10^{-3}	85 °C, 98% RH	0.39	This
PSM-1	1.64×10^{-1}	80 °C, 95% RH	0.107	Ref.[3]
BUT-8-(Cr)A	1.27×10^{-1}	80 °C, 100% RH	0.11	Ref.[4]
PCMOF2$^1/_2$(Tz)	1.17×10^{-1}	85 °C, 90% RH	0.22	Ref.[5]
PCMOF2$^1/_2$(Pz)	1.10×10^{-1}	85 °C, 90% RH	0.16	Ref.[5]
UIO-66-$(SO_3H)_2$	8.4×10^{-2}	80 °C, 90% RH	0.32	Ref.[6]
TfOH@MIL-101	8.0×10^{-2}	60 °C,15% RH	0.18	Ref.[7]
CPM-103a	5.8×10^{-2}	22.5 °C,98% RH	0.66	Ref.[8]
Fe-CAT-5	5.0×10^{-2}	25 °C, 98% RH	0.24	Ref.[9]
BUT-8-(Cr)	4.63×10^{-2}	80 °C, 100% RH	0.21	Ref.[4]
$[(Me_2NH_2)_3(SO_4)_2]_2[Zn_2(ox)_3]$	4.2×10^{-2}	25°C, 98% RH	0.13	Ref.[10]
PCMOF-10	3.55×10^{-2}	70°C, 95% RH	0.40	Ref.[11]
VNU-15	2.9×10^{-2}	95°C, 60% RH	0.22	Ref.[12]
COG-10P	2.3×10^{-2}	60°C,anhydrous	0.29	Ref.[13]
PCMOF2$^1/_2$	2.1×10^{-2}	85°C, 90% RH	0.21	Ref.[14]
MROF-1	1.72×10^{-2}	70°C, 97% RH	0.37	Ref.[15]
Im@Fe−MOF	1.21×10^{-2}	60°C, 98% RH	0.436	Ref.[16]
MIL-101-SO_3H	1.16×10^{-2}	80 °C, 100% RH	0.23	Ref.[4]
FJU-17	1.08×10^{-2}	100 °C	0.29	Ref.[17]
H_2SO_4@MIL-101	1.0×10^{-2}	150 °C, 0.13% RH	0.42	Ref.[18]
H_3PO_4@MIL-101	1.0×10^{-2}	140 °C, 1.1% RH	0.25	Ref.[18]
$(NH_4)_2(adp)[Zn_2(ox)_3]\cdot3H_2O$	8×10^{-3}	25 °C, 98% RH	0.63	Ref.[19]
PSM-2	4.6×10^{-3}	80 °C, 95% RH	0.292	Ref.[3]
Cu-TCPP MOF	3.9×10^{-3}	25°C, 98% RH	0.28	Ref.[20]
PCMOF-5	2.5×10^{-3}	60 °C, 98% RH	0.16	Ref.[21]
UiO-66(Zr)-$(CO_2H)_2$	2.3×10^{-3}	90 °C, 95% RH	0.17	Ref.[22]
β-PCMOF2	1.3×10^{-3}	85 °C, 90% RH	0.28	Ref.[14]
PCMOF-17	1.17×10^{-3}	25 °C, 40% RH	0.31	Ref.[23]

Section S3 Additional Structural Figures and Characterizations

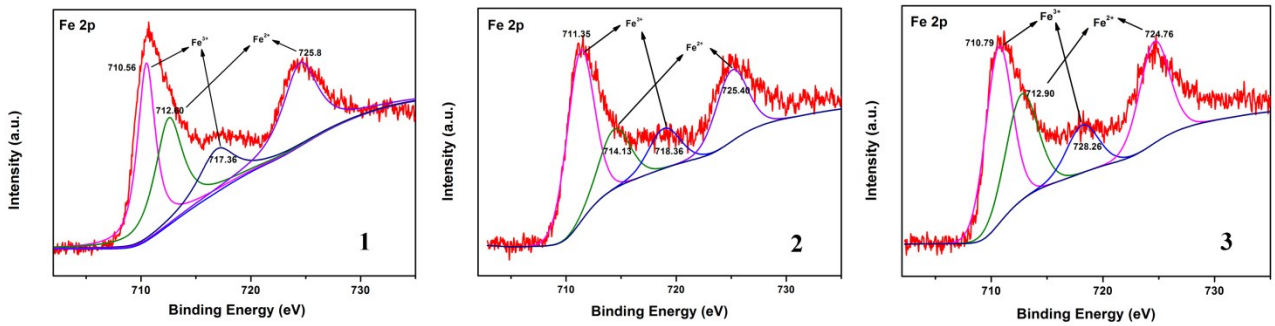

Fig. S1 X-ray photoelectron spectroscopy of **1-3**.

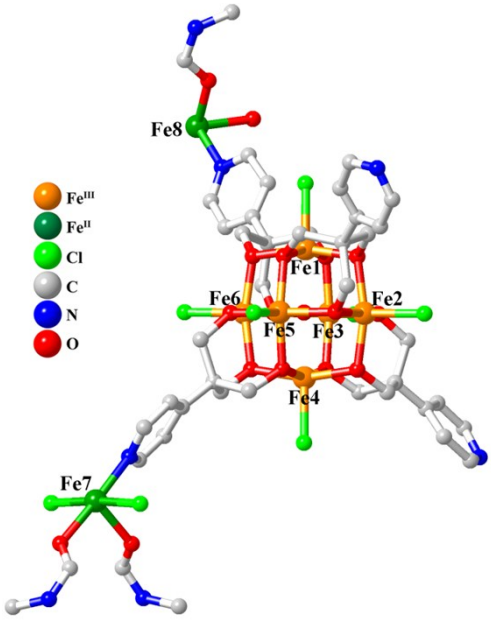

Fig. S2 The asymmetric unit of **1**.

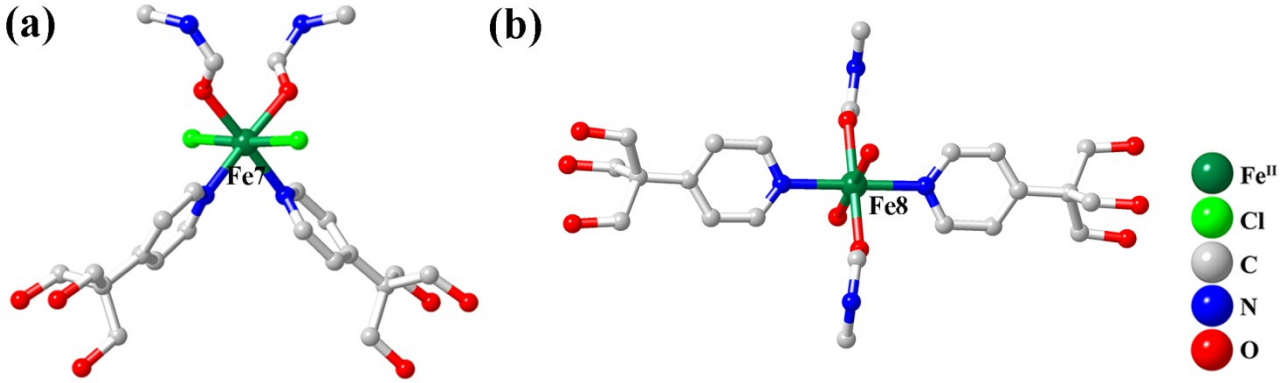

Fig. S3 The $\{FeCl_2L_2(NMF)_2\}$ fragment (a) and the $\{Fe(H_2O)_2L_2(NMF)_2\}$ fragment (b) in **1**.

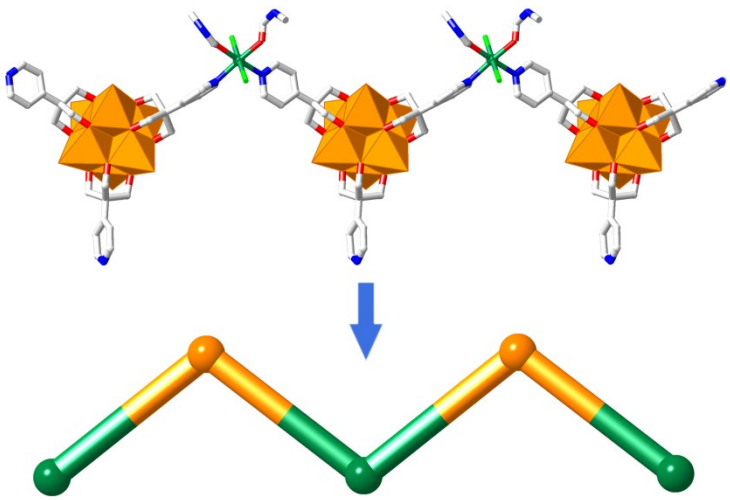

Fig. S4 The 1D infinite Z-shape chain in **1**.

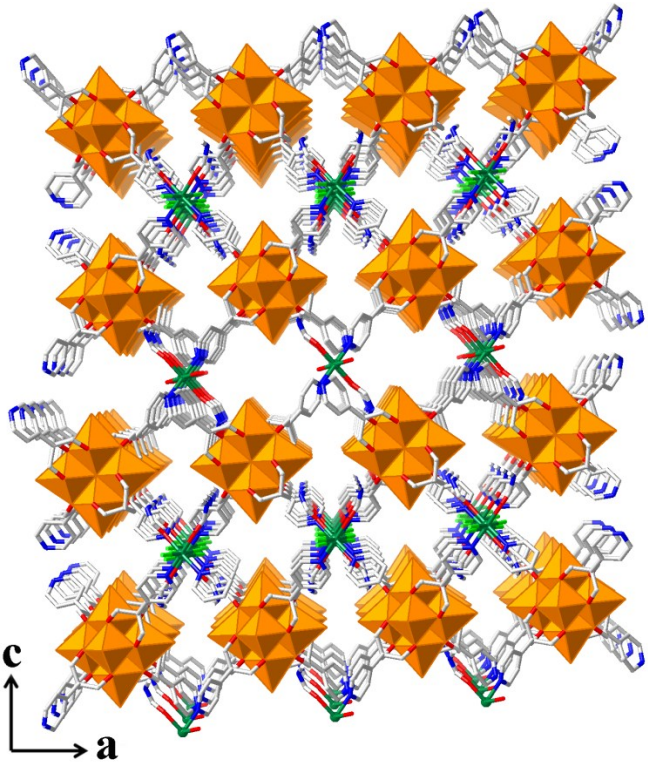

Fig. S5 The 1D channels in **1** along the *b*-axis.

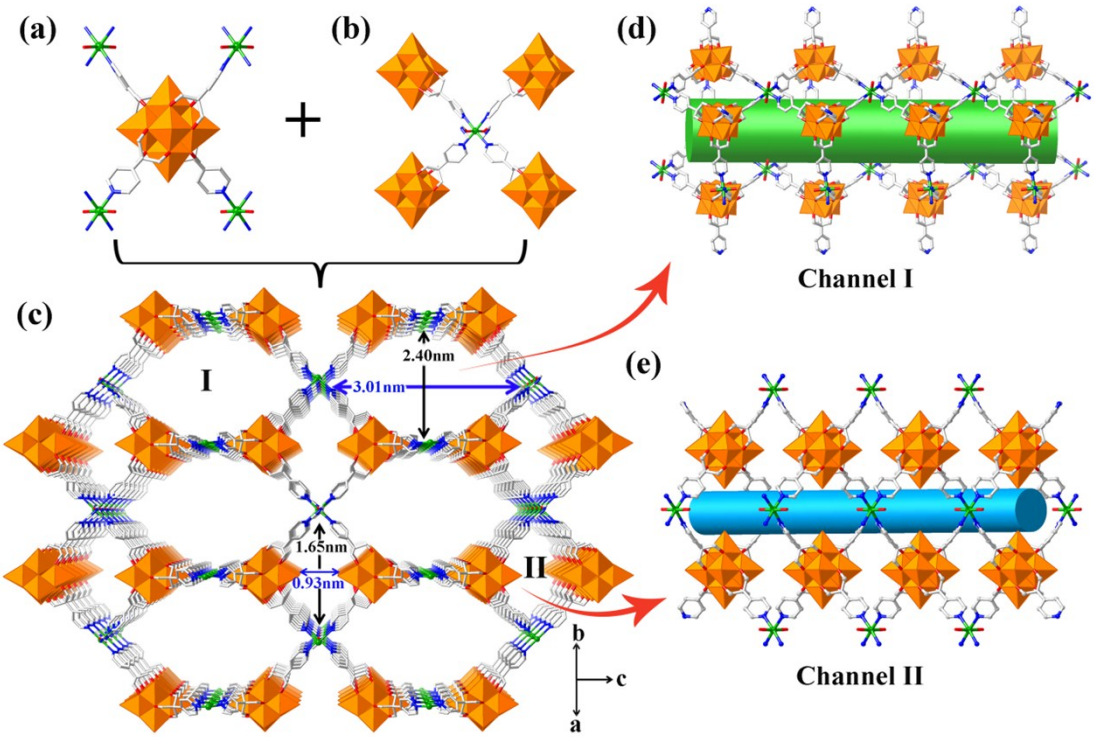

Fig. S6 (a) The 4-connected $\mathbf{Fe_6}$ cluster in **2**; (b) 4-connected Fe^{2+} ion in **2**; (c) the 3D framework of **2** based on $\mathbf{Fe_6}$ cluster and Fe^{2+} ions; (d) hexagonal channel I and (e) rhombic channel II in **2.**

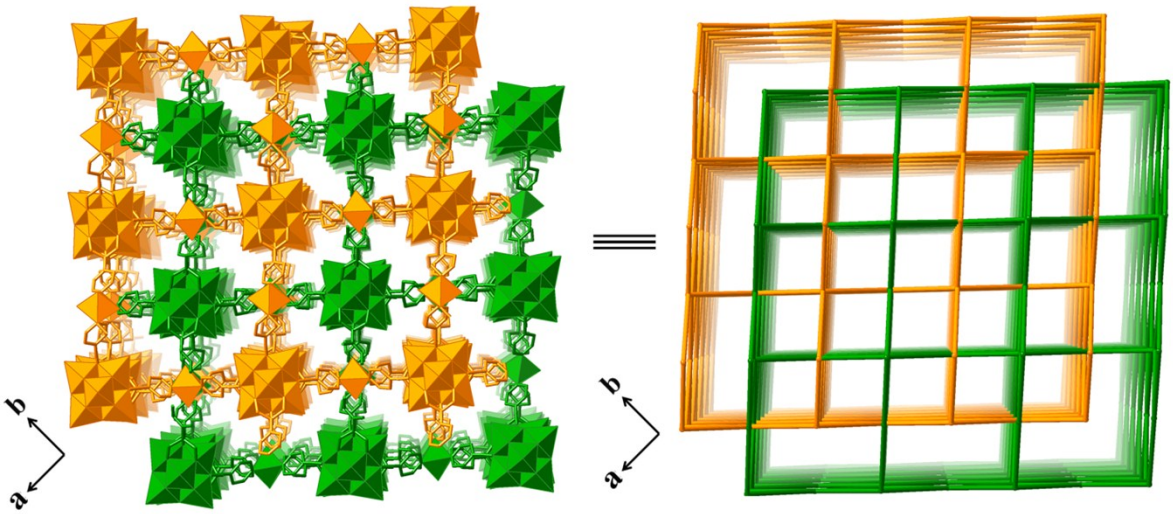

Fig. S7 (a) The pts-type 2-fold interpenetrated framework in **2**.

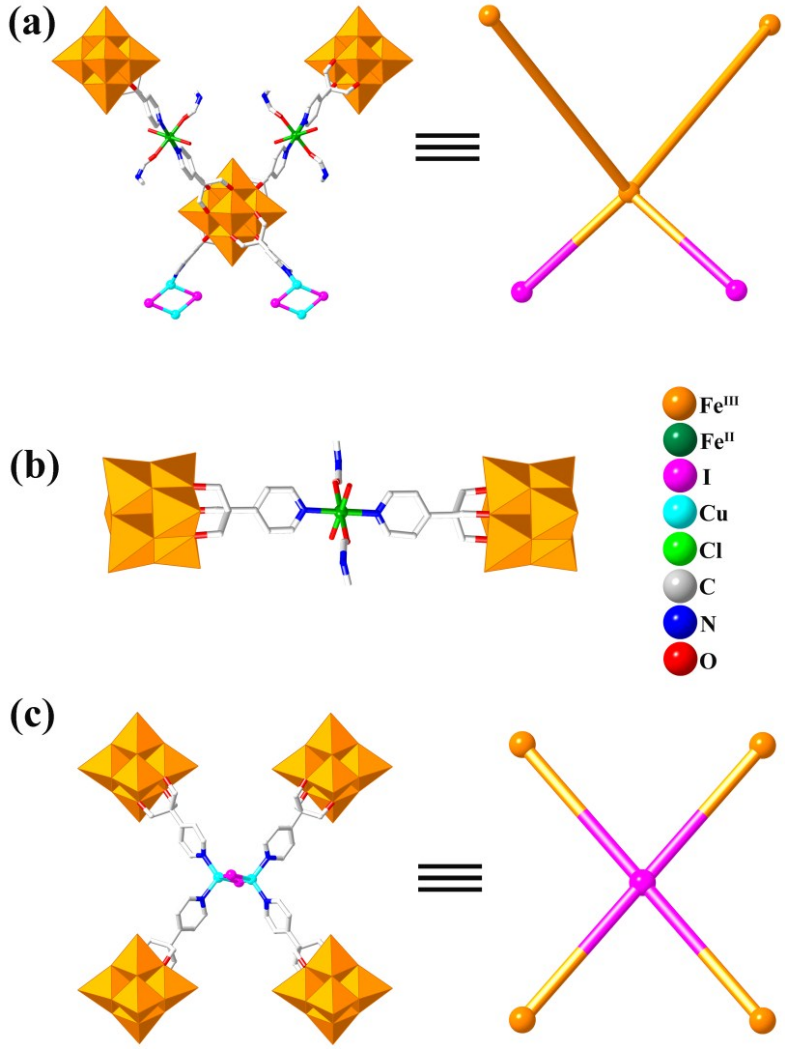

Fig. S8 (a) The 4-connected Fe_6 cluster and its node representation; (b) the $FeL_2(H_2O)_2(NMF)_2$ fragment connects two identical Fe_6 cluster; (c) the 4-connected Cu_2I_2 cluster and its node representation.

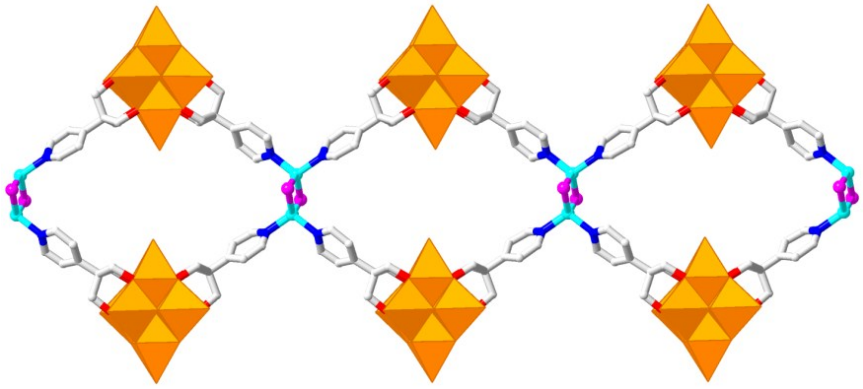

Fig. S9 View of the ribbon chain of **3**.

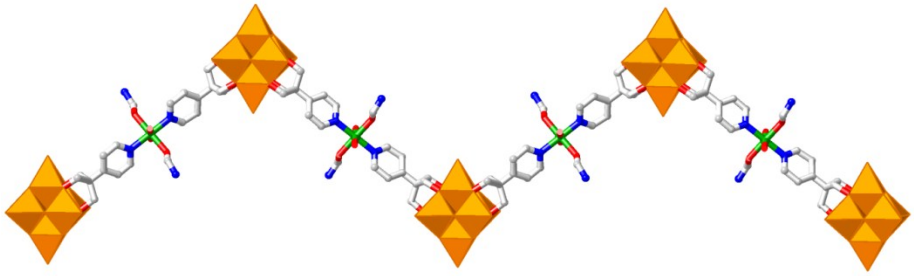

Fig. S10 View of the zigzag chain of **3**.

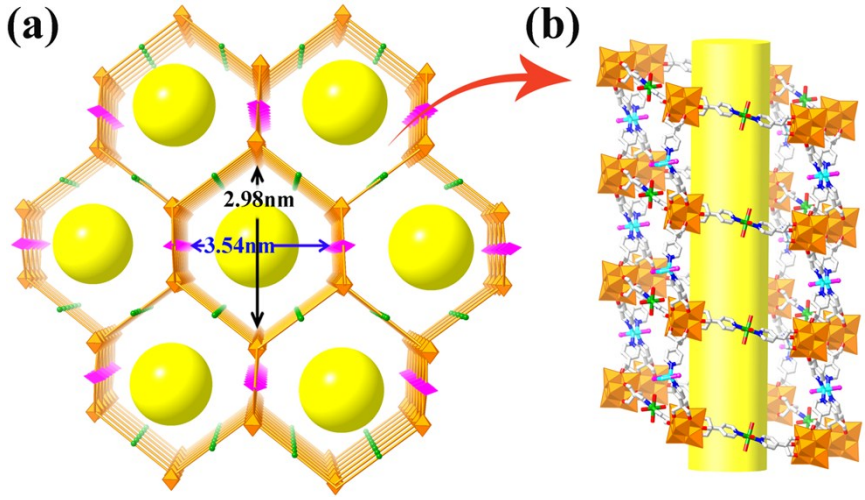

Fig. S11 The mog-type 3D framework of **3** based on Cu_2I_2 cluster, Fe_6 cluster and Fe^{2+} ions (a), showing a hexagonal nanometer size 1D channel (b).

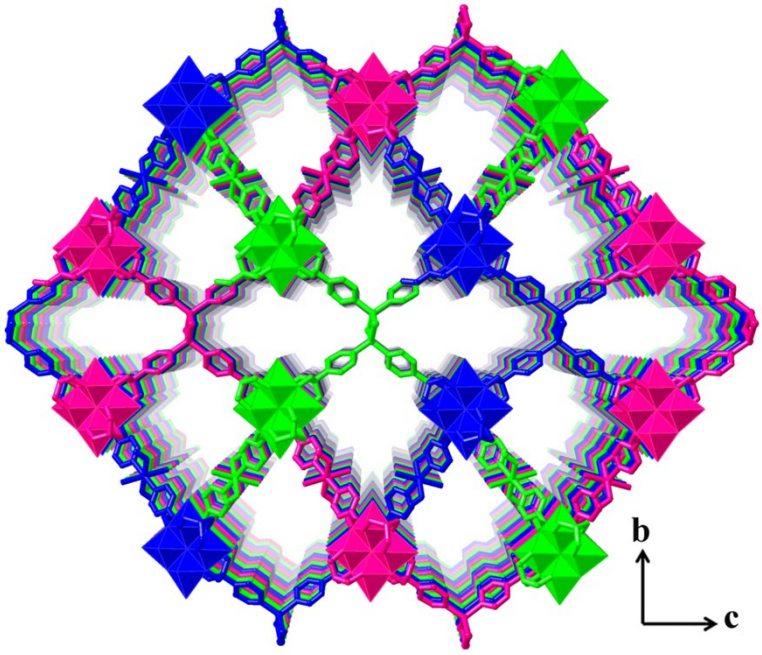

Fig. S12 The 3-fold interpenetrated framework of **3**.

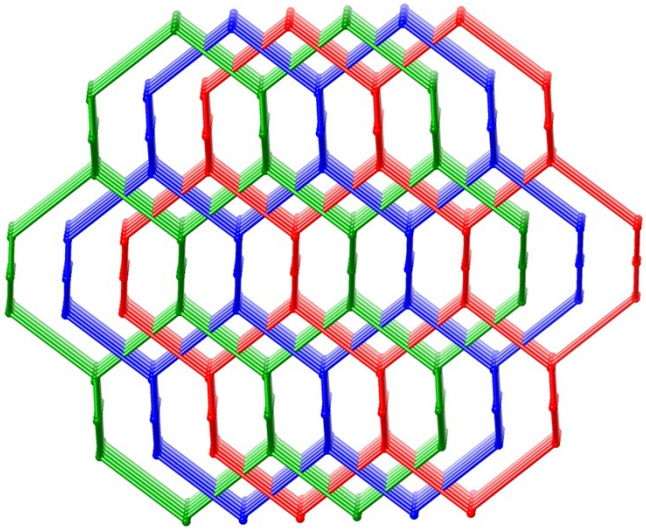

Fig. S13 The *mog*-type 3-fold interpenetrated framework in **3**.

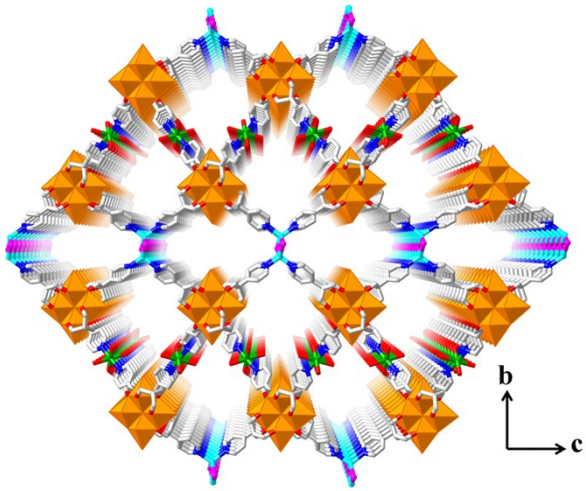

Fig. S14 The 3D framework of **3** along the *a* axis.

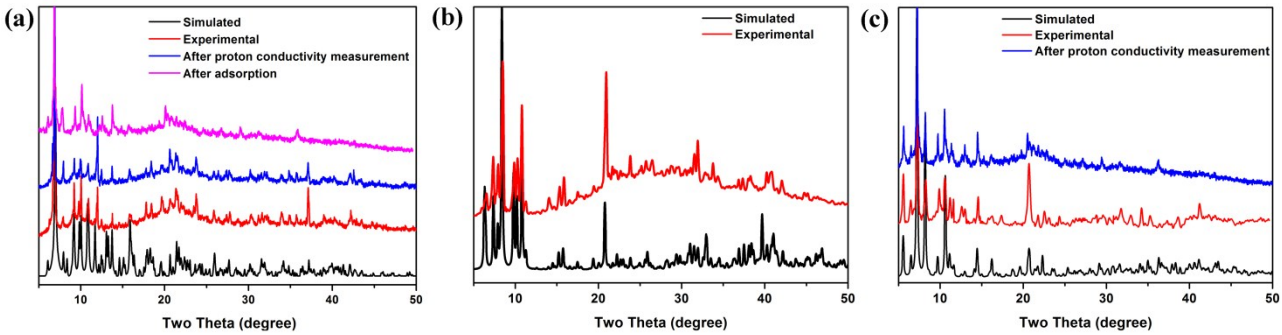

Fig. S15 Powder XRD patterns for **1** (a), **2** (b) and **3** (c).

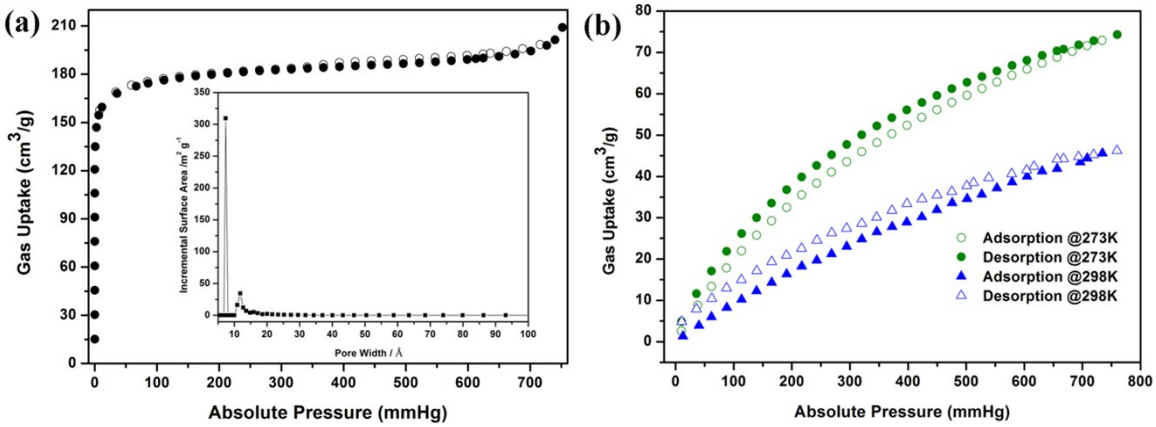

Fig. S16 (a) N_2 sorption isotherms at 77 K for **1**. Inset: Pore size distribution analyzed by a density functional theory (DFT) model. (b) CO_2 gas adsorption properties of **1** at 273 K and 298 K.

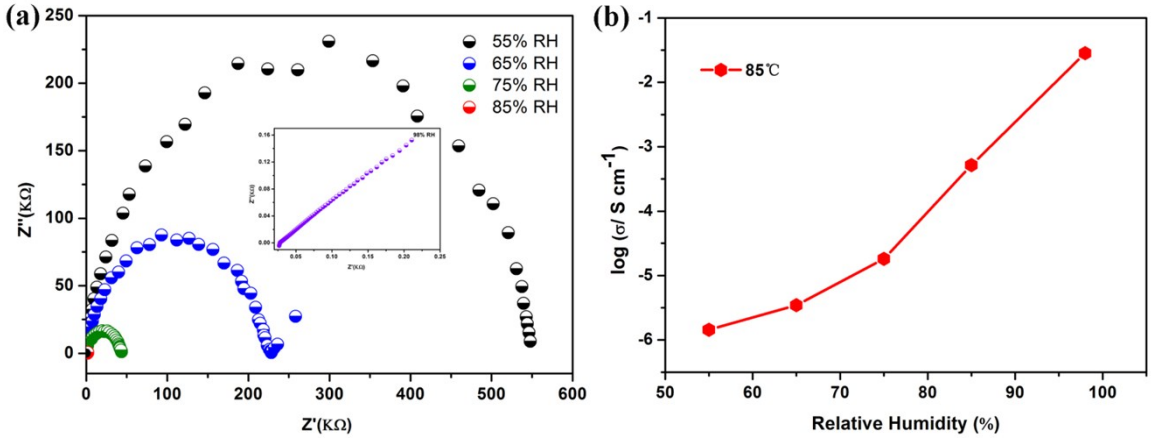

Fig. S17 (a) Impedance diagrams of **1** at 85 °C with different RHs. (b) Dependence of proton conductivity in **1** as a function of relative humidity at 85 °C.

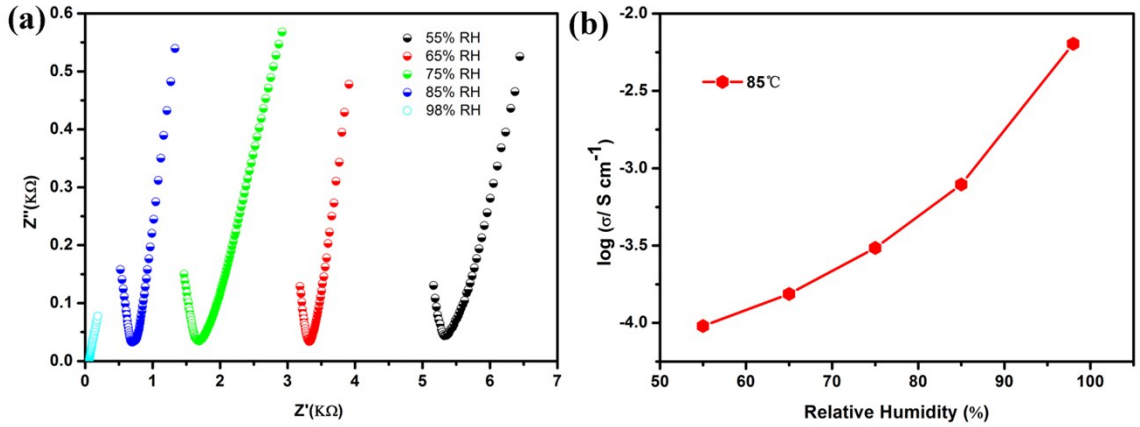

Fig. S18 (a) Impedance diagrams of **3** at 85 °C with different RHs. (b) Dependence of proton conductivity in **3** as a function of relative humidity at 85 °C.

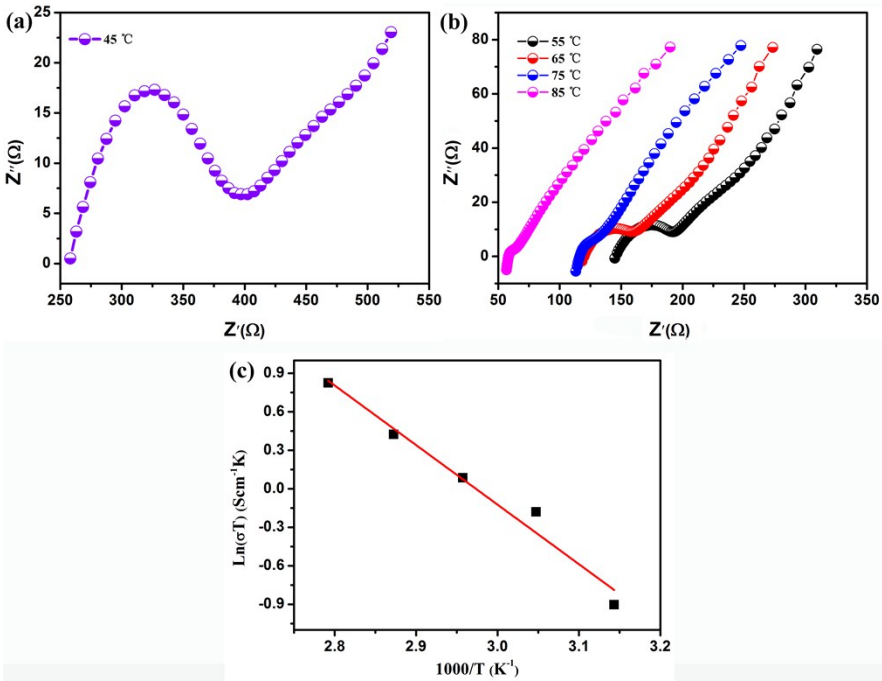

Fig. S19 (a) and (b) temperature-dependent impedance diagrams of **3** at 98% RH; (c) Arrhenius plots of **3**.

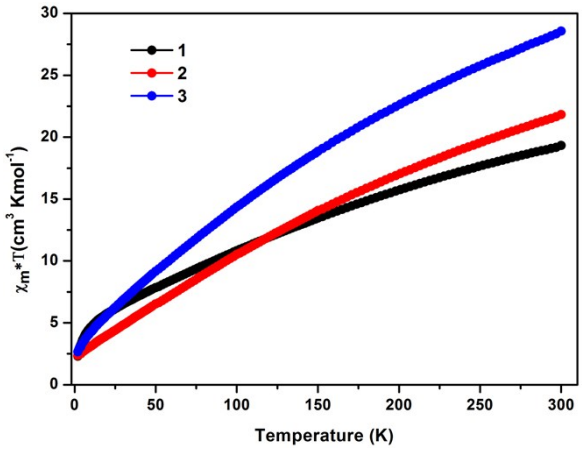

Fig. S20 Plot of $\chi_M T$ versus the temperature for **1-3** in the temperature range of 2-300K in an applied magnetic field of 1000 Oe.

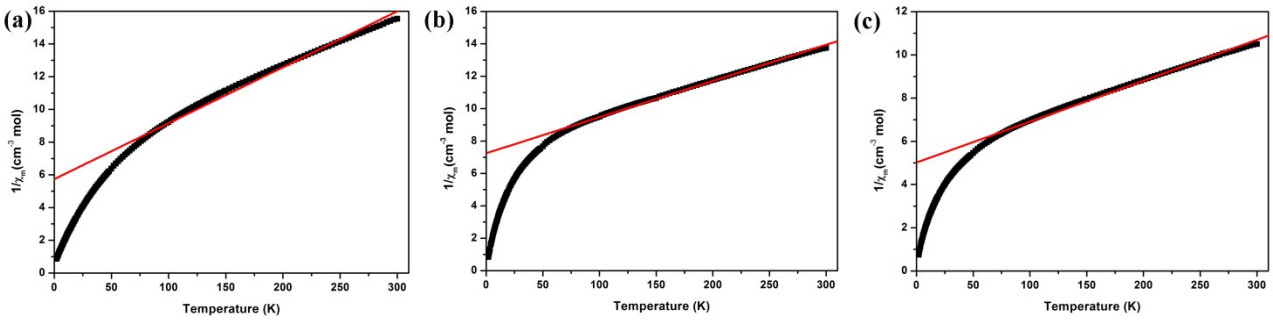

Fig. S21 Plot of $1/\chi_m$ versus the temperature for **1**(a), **2** (b) and **3** (c) in the temperature range of 2-300 K in an applied magnetic field of 1000 Oe.

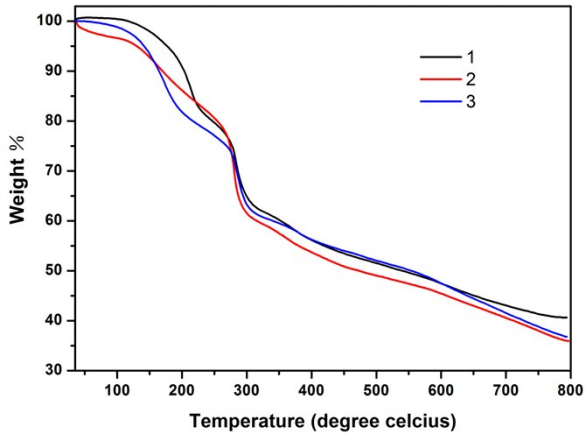

Fig. S22 TG curves of **1-3**.

REFERENCES

[1] D. Menozzi, E. Biavardi, C. Massera, F. P. Schmidtchen, A. Cornia and E. Dalcanale, *Supramol. Chem.*, 2010, **22**, 768.

[2] A. L. Spek, *Acta Crystallogr., Sect. C: Struct. Chem.*, 2015, **71**, 9.

[3] S. Mukhopadhyay, J. Debgupta, C. Singh, R. Sarkar, O. Basu and S. K. Das, *ACS Appl. Mater. Interfaces.*, 2019, **11**, 13423.

[4] F. Yang, G. Xu, Y. B. Dou, B. Wang, H. Zhang, H. Wu, W. Zhou, J. R. Li and B. L. Chen, *Nat. Energy.,* 2017, **2**, 877.

[5] S. Kim, B. Joarder, J. A. Hurd, J. F. Zhang, K. W. Dawson, B. S. Gelfand, N. E. Wong and G. K. H. Shimizu, *J. Am. Chem. Soc.* , 2018, **140**, 1077.

[6] W. J. Phang, H. Jo, W. R. Lee, J. H. Song, K. Yoo, B. Kim and C. S. Hong, *Angew. Chem. Int. Ed.,* 2015, **54**, 5142.

[7] D. N. Dybtsev, V. G. Ponomareva, S. B. Aliev, A. P. Chupakhin, M. R. Gallyamov, N. K. Moroz, B. A. Kolesov, K. A. Kovalenko, E. S. Shutova and V. P. Fedin, *ACS Appl. Mater. Interfaces*., 2014, **6**, 5161.

[8] Q. G. Zhai, C. Y. Mao, X. Zhao, Q. P. Lin, F. Bu, X. T. Chen ,X. H. Bu and P. Y. Feng, *Angew. Chem. Int. Ed.,* 2015, **54**, 7886.

[9] N. T. T. Nguyen, H, Furukawa, F. Gandara, C. A. Trickett, H. M. Jeong, K. E. Cordova and O. M. Yaghi, *J. Am. Chem. Soc.,* 2015, **137**, 15394.

[10] S. S. Nagarkar, S. M. Unni, A, Sharma, S. Kurungot and S. K. Ghosh, *Angew. Chem. Int. Ed.,* 2014, **53**, 2638.

[11] P. Ramaswamy, N. E. Wong, B. S. Gelfand and G. K. H. Shimizu, *J. Am. Chem. Soc.,* 2015, **137**, 7640.

[12] T. N. Tu, N. Q. Phan, T. T. Vu, H. L. Nguyen, K. E. Cordova and H. Furukawa, *J. Mater. Chem. A,* 2016, **4**, 3638.

[13] H. Zhong, Z. H. Fu, J. M. Taylor, G. Xu and R. H. Wang, *Adv. Funct. Mater.* 2017, **27**, 1701465.

[14] S. Kim, K. W. Dawson, B. S. Gelfand, J. M. Taylor and G. K. H. Shimizu, *J. Am. Chem. Soc.,* 2013, **135**, 963.

[15] Y. H. Han, Y. X. Ye, C. B. Tian, Z. J. Zhang, S. W. Du and S. C. Xiang, *J. Mater. Chem. A,* 2016, **4**, 3638.

[16] F. M. Zhang, L. Z. Dong, J. S. Qin, W. Guan, J. Liu, S. L. Li, M. Lu, Y. Q. Lan, Z. M. Su and H. C. Zhou, *J. Am. Chem. Soc.,* 2017, **139**, 6183.

[17] L. Z. Liu, Z. Z. Yao, Y. X. Ye, Q. J. Lin, S. M. Chen, Z. J. Zhang and S. C. Xiang, *Cryst. Growth Des.,* 2018, **18**, 3724.

[18] V. G. Ponomareva, K. A. Kovalenko, A. P. Chupakhin, D. N. Dybtsev, E. S. Shutova and V. P. Fedin, *J. Am. Chem. Soc.,* 2012, **124**, 15640.

[19] M. Sadakiyo, T. Yamada and H. Kitagawa, *J. Am. Chem. Soc.,* 2009, **131**, 9906.

[20] G. Xu, K. Otsubo, T. Yamada, S. Sakaida and H. Kitagawa, *J. Am. Chem. Soc.,* 2013, **135**, 7438.

[21] J. M. Taylor, K. W. Dawson and G. K. H. Shimizu, *J. Am. Chem. Soc.* , 2013, **135**, 1193.

[22] D. D. Borges, S. Devautour-Vinot, H. Jobic, J. Ollivier, F. Nouar, R. Semino, T. Devic, C. Serre, F. Paesani and G. Maurin, *Angew. Chem. Int. Ed.,* 2016, **55**, 3919.

[23] B. Joarder, J. B. Lin, Z. Romero and G. K. H. Shimizu, *J. Am. Chem. Soc.,* 2017, **139**, 7176.